Barcelona '10

F021

Detetection of Mechanical Failure During Hyraulic Fracturing Through Passive Seismic Microseismic Monitoring

A. De La Pena* (Microseismic Inc.), L. Eisner (Microseismic Inc.), M.P. Thornton (Microseismic Inc.) & S. Williams-Stroud Ph.D (Microseismic Inc.)

SUMMARY

Microseismic monitoring is extensively used for detection of microseismic events induced by hydraulic fracture stimulation and detected microseismic events are assumed to be caused by fracture growth in a formation. However, not all microseismic events are created equal as some events might be caused by mechanical changes in the completion. Source mechanism analysis of the micro-earthquakes proved to be an excellent tool to discriminate between the two types of events. We show a non-shear event of stage 4 that seems to be related to a mechanical failure on the casing, as the energy radiation pattern is mostly horizontal and sub parallel to the horizontal section of the well and consistent with tensile opening. Fracture related events are well explained by double couple dip-slip mechanisms occurred at time of fracture propagation while pumping.

Introduction

Microseismic monitoring is extensively used for detection of microseismic events induced by hydraulic fracture stimulation. Usually, all detected microseismic events are assumed to be caused by fracture growth in a formation. Recently microseismic monitoring was also used to identify microseismic events caused casing expansion in steam injection (Maxwell et.al., 2008). Such identification allowed the operator to better identify events that represent fracture geometry instead of casing expansion. Note that microseismic events caused by hydraulic fracture growth as well as mechanical events in the vicinity of the wellbore both radiate P- and S-waves. Maxwell et.al. (2008) differentiate between these events by comparing P- and S-wave amplitude ratios of different events. This approach allows a limited ability to differentiate between microseismic events, but does not provide information on the nature of mechanical failure and may often fail when a single monitoring well is used because of the limited aperture. We propose use of source mechanisms of individual events to differentiate between hydraulic fracture and mechanical microseismic events. The source mechanism inversion uses P-wave (or S-wave or both) amplitudes to determine volumetric and shear part of the failure that caused a microseismic event. The inversion for volumetric part is not possible from a limited number of receivers (such as a single vertical monitoring borehole, see Vavryčuk, 2007 for more details), which is probably the main reason why this approach was not used until recently. We use passive microsesimic monitoring from the surface with receivers distributed in multiple azimuths and offsets to constrain source mechanisms of microseismic events induced during hydraulic fracturing. In this case study, microseismic events induced by the growth of the hydraulic fracture have very nearly pure shear mechanisms with failure plane closely aligned with expected SH maximum, while mechanical event has significant volumetric component with tensile opening along the horizontal well.

Method

We use source mechanism inversion from the surface data based on a least squares inversion of the observed P-wave amplitudes recorded on vertical component. The inversion algorithm uses the same data to invert the full moment inversion (i.e. including the volumetric part of the source mechanism), and double-couple (shear) mechanism. In both cases we assume a point source. The moment tensor representing the source mechanism can be inverted from a point source relationship between observed displacements on vertical component A and moment tensor components M_{jk}:

$$A = G_{3j,k} M_{jk} \ , \tag{1}$$

Where $G_{3j,k}$ are vertical components of the Green's function derivative and Einstein's summation rules applies (Aki and Richard, 1980). Equation (1) can be inverted by either least squares (Sipkin, 1982) or a grid search (grid search is possible only for pure shear source mechanism as non-shear source mechanisms have infinite number of possible combinations of M_{jk}).

Although in principle it is possible to use multiple waves observed at the surface (such as P- and S-waves), amplitudes of direct P-waves on vertical receiver components are used for inversion of moment tensor in this study as the aperture and distribution of the array allows a robust solution. The Green's function derivatives of a homogeneous isotropic medium with correction for free surface and attenuation can be written as:

$$G_{3j,k} = \frac{M_0}{4\pi\rho r c^3} \gamma_3 \gamma_j \gamma_k 2 e^{-\frac{\pi r f}{cQ}} \ , \tag{2}$$

Where ρ is density, r is the distance between source and receiver, c is P-wave velocity, γ_i are components of a unit vector from source to the receiver, f is dominant frequency of the signal and Q is attenuation coefficient. The exponential term in equation (2) accounts for attenuation and is equal to 1 if attenuation is neglected. The factor of 2 before the exponential term approximates the free surface reflection as the observed waves are both direct and reflected P-waves (i.e., assuming no P-to-S conversion at the free surface). The linear distance r dependence of the moment represents spherical

divergence and can be directly derived from energy conservation. For heterogeneous medium (e.g., 1D medium) the term rc^3 is replaced by geometrical spreading which accounts for all transmission coefficients. The attenuation term in heterogeneous medium becomes only slightly more complex as the term $r/(cQ)$ is replaced by t*, also known as effective attenuation.

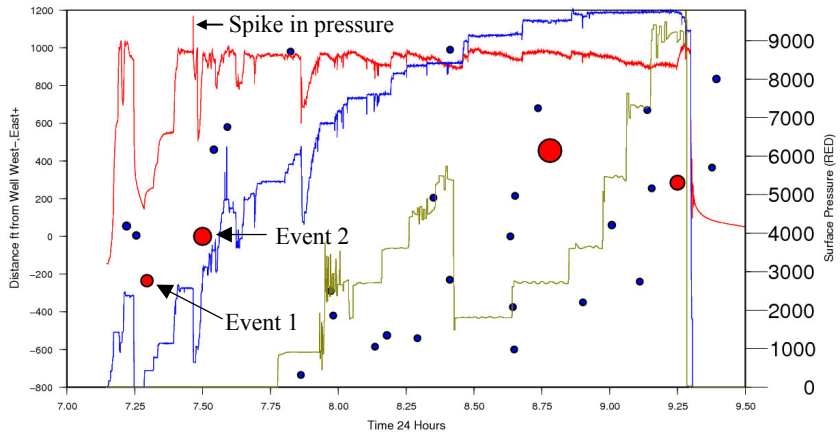

Figure 1 *Plot representing the timing of the events recorded with respect to the engineering parameters: pressure (red line), slurry rate (blue line, maximum 100bpm) and proppant (green line, maximum 2.5lb/gal).Red circles represent events with Moment Magnitude larger than 0, and blue circles are events with magnitudes smaller than 0.*

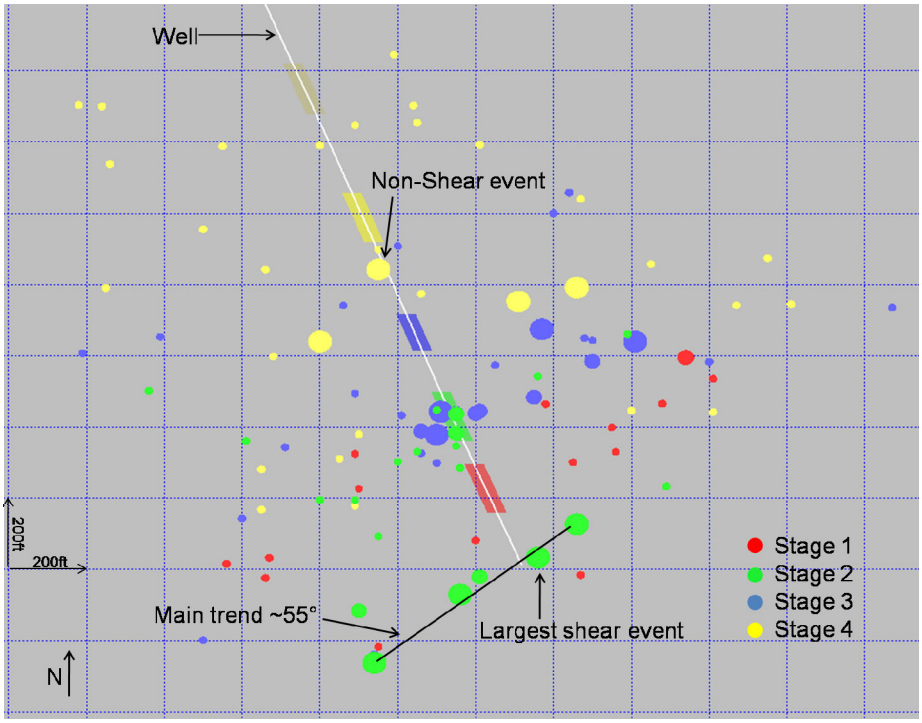

Figure 2 *Map view of the located events on the first 4 stages of the fracture treatment. Events are color coded by treated stage.*

Case Study

The hydraulic fracture stimulation was carried out in the Marcellus shale in southwest Pennsylvania, U.S.A. The surface array, FracStar® consisted of 1013 vertical component receivers with 12 geophones per receiver. There were 7 stages treated by perf and plug system with an average duration of 2.5 hrs per stage. A total of 70027 bbl of fracturing fluid was injected at maximum 100 bpm injection rate (see Figure 1 for an example of the injection schedule on stage 4). Each stage consisted of fracture fluid pad followed by injection of proppant, totalling 3201124 lbs for the entire frac. This study will focuses on microseismic events induced during the successful stages 1-4 of the hydraulic fracturing that totalled ~8800 bbl of fluid, 330000 lbs of proppant at an average of 8500 Psi injection pressure per stage (the remaining 3 stages were not considered a successful stimulation). At the beginning of stage 4 a steel ball is dropped to isolate the current perforation interval from the

previously treated sections. A microseismic event (event 1) was observed at the time of Instantaneous Shut in Pressure (ISIP) and the timing of this event is shown at Figure 1. After this step in the stage pumping is resumed and a sudden increase in pressure was observed about 15 minutes after event 1 (ISIP). Immediately after the spike in pressure the rate was reduced until the pressure came back to normal 8500 psi. Then the rate was increased until the pressure rose to ~8700 Psi when around 7:29 hrs a 2400 Psi drop in pressure occurred and a large event (event 2) was detected (Figure 1). The detailed analysis of this event 2 with respect to the rest of the large events detected during the first four stages reveals a different source mechanism for this event.

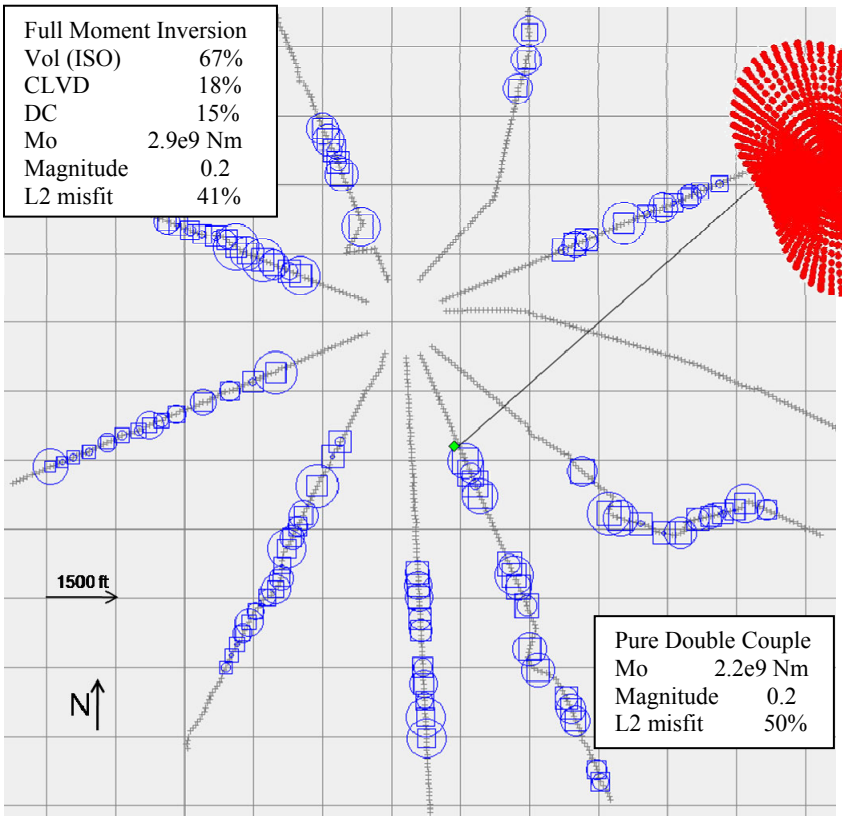

Figure 3 *Map view of the surface array showing the stations where first P-wave arrival was reliably detected (only every third station is shown for this size of Figure). The green diamond represents surface projection of located microseismic event (epicentre). Table in the upper left and lower right corners summarize results of the full moment and pure double couple inversion respectively. The blue circles and squares represent the observed and calculated amplitudes of P-wave arrivals, respectively. Blue color represents motion up. Grey crosses without circle/square represent receivers where P-wave arrival was not reliably determined. Full moment inversion result: Vol (ISO), CLVD, DC, M_o, L2 misfit stand for volumetric component, Compensated Linear Vector Dipole, Double Couple, Moment and Least squares misfit respectively. The red vectors show a map view of the P-wave first motion radiation pattern associated with the non-shear event, red color represents motion out. Notice that energy is mostly radiated in a northwest-southeast direction sub parallel to the wellbore (Figure 2).*

Figure 2 shows map view of events located during stages 1-4. As discussed earlier a large event with magnitude 0.2 was observed very close to the stimulation interval of the stage 4. This event had unusual radiation pattern illustrated in Figure 3. The radiation pattern did not show any polarity reversal of the P-wave arrivals on 9 arms of the FracStar® monitoring array representing nearly half of the radiated energy. For comparison Figure 4 shows a typical radiation pattern observed for microseismic events located further away from the treatment well. Note that P-wave amplitudes in Figure 4 decline as they approach the nodal line where polarity of the P-wave arrivals changes. This is not observed in Figure 3 for the event seemingly associated with a mechanical failure.

We have carried out source mechanism inversion described in Method Section for both events. The event associated with the mechanical failure is significantly better explained by a non-shear mechanism (misfit of 41% with non-shear mechanism is better than misfit of 50% of shear only mechanism). The inversion for non-double couple part of the source mechanism is well constrained even with lower number of the reliable arrivals giving a condition number of the least square inversion of approximately 30 (500 is usually considered to be limiting number for this kind of

inversion). The inverted mechanism can be explained by mostly tensile opening in a horizontal direction as shown in Figure 3 (radiation pattern plot in upper right corner). Contrary to this, the frac event mechanism shown in Figure 4 is very well explained by shear-only mechanism with two fault planes, one nearly horizontal and one nearly vertical striking approximately 55° east as observed in the trend of detected microseismicity (see Figure 2).

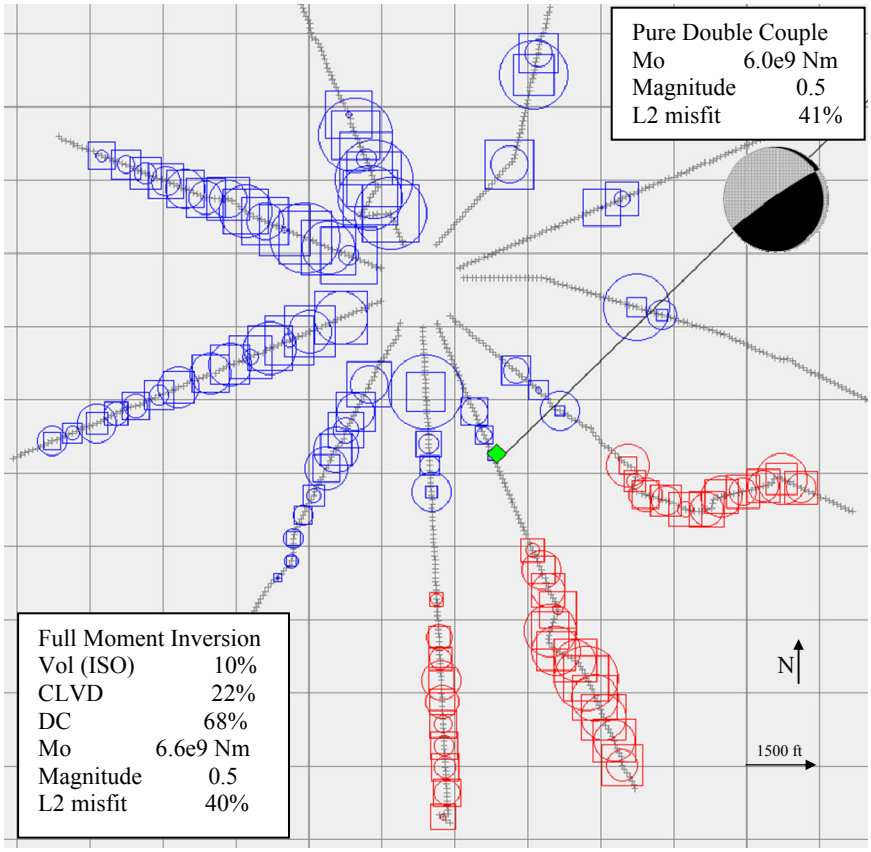

Figure 4 *Map view of the surface array showing the stations where first P-wave arrival was reliably detected for the shear event representing fracture associated microseismic event. The blue and red circles represent the observed P-wave amplitudes, blue represents first motion up, red represent first motion down. See Figure 3 for more details of the figure caption. The mechanism is represented in the upper right corner by lower hemisphere projection.*

Conclusions

Source mechanism analysis of the micro-earthquakes proved to be an excellent tool to discriminate non-shear (Figure 3) and shear (Figure 4) events. The non-shear event of stage 4 seems to be related to the mechanical failure on the casing, as the energy radiation pattern is mostly horizontal and sub parallel to the horizontal section of the well. Furthermore, the event occurs in very close vicinity of the borehole and at time of the significant increase of surface pressure. One possible explanation is that the steel ball used to isolate stage 4 shattered resulting in a sudden drop in pressure. Shear events are well explained by double couple dip-slip mechanisms occurred at time of fracture propagation while pumping.

References

Aki and Richards, 1980: Quantitative seismology. Theory and Methods. Freeman, San Francisco, Calif.

Maxwell, S.C., J. Du, J. Shemeta, U. Zimmer, N. Boroumand and L. Griffin, 2008: Passive seismic and surface deformation monitoring of steam injection. First Break, Vol 26, pp 53-59

Sipkin, S.A., 1982: Estimation of earthquake source parameters by the inversion of waveform data: synthetic waveforms, Phys. Earth planet. Inter., 30, 242-259.

Vavryčuk, V., 2007. On the retrieval of moment tensors from borehole data. Geophys. Prospect. 55 (3), 381–391.